Recursive Deep Inverse Reinforcement Learning

Paul Ghanem
Department of Computer Engineering
Northeastern University
Boston, MA 02115
ghanem.p@northeastern.edu

Owen Howell
Boston Dynamics AI Institute
Boston, MA 02142
howell.o@northeastern.edu

Michael Potter
Department of Computer Engineering
Northeastern University
Boston, MA 02115
potter.m@northeastern.edu

Pau Closas
Department of Computer Engineering
Northeastern University
Boston, MA 02115
pau.closas@northeastern.edu

Alireza Ramezani
Department of Computer Engineering
Northeastern University
Boston, MA 02115
a.ramezani@northeastern.edu

Deniz Erdogmus
Department of Computer Engineering
Northeastern University
Boston, MA 02115
D.erdogmus@northeastern.edu

Tales Imbiriba
Department of Computer Engineering
University of Massachusetts
Boston, MA 02125
tales.imbiriba@umb.edu

Reviewed on OpenReview: https://openreview.net/forum?id=bYItLUU135

Abstract

Inferring an adversary's goals from exhibited behavior is crucial for counterplanning and non-cooperative multi-agent systems in domains like cybersecurity, military, and strategy games. Deep Inverse Reinforcement Learning (IRL) methods based on maximum entropy principles show promise in recovering adversaries' goals but are typically offline, require large batch sizes with gradient descent, and rely on first-order updates, limiting their applicability in real-time scenarios. We propose an online Recursive Deep Inverse Reinforcement Learning (RDIRL) approach to recover the cost function governing the adversary actions and goals. Specifically, we minimize an upper bound on the standard Guided Cost Learning (GCL) objective using sequential second-order Newton updates, akin to the Extended Kalman Filter (EKF), leading to a fast (in terms of convergence) learning algorithm. We demonstrate that RDIRL is able to recover cost and reward functions of expert agents in standard and adversarial benchmark tasks. Experiments on benchmark tasks show that our proposed approach outperforms several leading IRL algorithms.

1 Introduction

Inverse Optimal Control (IOC) and Inverse Reinforcement Learning (IRL) aim to infer parameterized cost and reward functions in optimal control and reinforcement learning problems, respectively, from observed state-control data. This data is assumed to be generated by an expert following an optimal policy that either minimizes a cost function or maximizes a reward function.

Previous IRL approaches have included maximum-margin approaches (Abbeel & Ng, 2004), and probabilistic approaches such as Ziebart et al. (2008). In this work, we build on the maximum entropy IRL framework presented previously (Ziebart et al., 2008). In this framework, training consists of two nested loops. The inner loop approximates the optimal control policy for a hypothesized cost function, while the outer loop minimizes a negative log-likelihood cost function (Ziebart et al., 2008), constructed by sampling a full trajectory from the inner loop's optimal control policy and by using the expert trajectory that is observed from the expert.

Due to this nested structure, training under the maximum entropy deep IRL in an online fashion becomes very challenging since inner and outer loops need long trajectories and large batch sizes to converge. Available IRL approaches exploit the fact that it is often feasible to store and process entire state and control sequences in batches (Molloy et al., 2018). In real-time settings with memory, latency and compute constraints, this is generally not feasible.

Recursive optimization strategies such as Extended Kalman Filter (EKF) sequentially minimize a loss function that is a summation of mean square error of observed and estimated states, and mean squared error of the estimated states and their predicted values produced by assumed model dynamics (Humpherys et al., 2012; Ghanem et al., 2023). Hence, EKF cannot be naively leveraged to optimize the negative log-likelihood function (Ziebart et al., 2008) since the log of summation term could not be optimized sequentially. Recent works have proposed moment-matching approaches (Swamy et al., 2021; Zeng et al., 2022; 2025), leading to objective functions that have a simple summation form, making them more suitable for online adaptive learning. However, they are not explicitly derived from maximum entropy IRL, and prior formulations have not been optimized in an online setting.

To overcome this limitation, we require a reformulation of the maximum entropy objective into a structure amenable to recursive optimization. To address this gap, we show that the moment matching loss function introduced in Swamy et al. (2021) provides an upper bound for the negative log-likelihood objective of maximum entropy IRL (Finn et al., 2016b; Ziebart et al., 2008). We then propose a recursive optimization algorithm that minimizes the moment matching loss using expert demonstrations and sampled trajectories from the inner optimal control policy. This approach alleviates the need to optimize the negative log-likelihood cost function only after collecting all trajectories from the inner-loop policy and the expert. Instead, it enables incremental optimization, processing each expert observation as it arrives.

The main contribution of this work is a deep maximum entropy online IRL algorithm, Recursive Deep Inverse Reinforcement Learning (RDIRL), that learns nonlinear cost and reward functions parameterized by neural networks directly from expert demonstrations as they arrive. Unlike previous deep learning approaches, our method updates the inner control policy after each new expert sample, enabling online adaptation of policies. By processing state–action pairs sequentially, without storing or batching entire trajectories, RDIRL is well-suited for real-time applications with memory and latency constraints. Moreover, because the policy and cost updates occur incrementally, our approach converges significantly faster than competing IRL methods. We validate our approach in simulated benchmark tasks, demonstrating that it outperforms leading IRL methods.

2 Related Work

IRL, also known as IOC (Finn et al., 2016b), aims to learn reward or cost functions from expert agents operating under optimal control or reinforcement learning policies. Several IOC methods have been developed to recover finite-horizon optimal control cost functions, including approaches based on Karush-Kuhn-Tucker (KKT) conditions (Zhang et al., 2019b;a; Puydupin-Jamin et al., 2012), Pontryagin's minimum principle (Molloy et al., 2022; 2020; Jin et al., 2020), and the Hamilton-Jacobi-Bellman equation (Pauwels et al., 2014; Hatz et al., 2012).

These methods typically follow a two-stage process: first, a feedback gain matrix is computed from state and control sequences using system identification techniques, and second, linear matrix inequalities are solved to recover the objective-function parameters from the feedback gain matrix. Online variations of IOC methods based on the Hamilton-Jacobi-Bellman equation (Zhao & Molloy, 2024; Molloy et al., 2018; 2020; Self et al., 2020c;a;b) have also been developed. However, both offline and online versions of these methods are generally limited to simple parameter estimation, assume partial knowledge of the expert's cost function, and do not incorporate deep neural network (Deep Neural Network (DNN)) representations of cost functions.

IRL approaches have also been proposed based on maximum margin (Abbeel & Ng, 2004; Ratliff et al., 2006) and maximum entropy (Ziebart et al., 2008; Boularias et al., 2011). Among these, maximum entropy IRL, as introduced by Ziebart et al. (2008), has become one of the leading approaches. In this framework, optimization seeks to find reward or cost function parameters that maximize the likelihood of the observed expert trajectory under a maximum entropy distribution. This involves estimating a partition function from samples drawn from a background distribution that represents a control policy (Finn et al., 2016a; Fu et al., 2017), which is dependent on a parameterized cost function. The control policy may range from reinforcement learning (Ho & Ermon, 2016; Fu et al., 2017) to receding horizon optimal control (Xu et al., 2022).

Building on maximum entropy IRL, feature-based methods (Hadfield-Menell et al., 2016; Wu et al., 2020) model the reward function as an inner product between a feature vector f and a parameter vector θ. These methods have been successfully implemented, with the feature characteristics and parameter vector size typically chosen to match the true cost function structure. However, they assume some structural knowledge of the expert's cost function or domain knowledge (Finn et al., 2016b). Online versions of feature-based maximum entropy IRL have also been developed (Rhinehart & Kitani, 2018; Arora et al., 2021), but they have not yet been extended to include a DNN parameterization of the reward and cost functions.

Similarly, maximum entropy IRL with deep learning representations of the reward function has been successfully implemented (Wulfmeier et al., 2015). These methods, which leverage DNNs for complex reward functions, have gained popularity and become widely used (Finn et al., 2016b; Wulfmeier et al., 2015; Ho & Ermon, 2016; Xu et al., 2019; 2022; Fu et al., 2017; 2019; Yu et al., 2019). As a result, they have emerged as leading IRL approaches, outperforming feature-based methods (Finn et al., 2016b; Xu et al., 2022; Ho & Ermon, 2016).

In this work, we propose a new online IRL method based on the maximum entropy framework (Ziebart et al., 2008; Ziebart, 2010). Unlike other online approaches (Molloy et al., 2018; Self et al., 2020c;b; Molloy et al., 2020; Rhinehart & Kitani, 2018; Arora et al., 2021), the proposed methodology allows the cost and reward functions to be parameterized using deep neural networks. Our approach is mostly related to the algorithm introduced by Finn et al. (2016a), which minimizes a negative log-likelihood function and uses

Model Predictive Path Integral Control (MPPI) (Xu et al., 2022) as the inner control policy. However, unlike prior work, we recursively adapt the sampling distribution representing the inner control policy each time an expert demonstration is observed.

To summarize, our proposed method is the first to combine several key features into a single effective algorithm. It can learn adversarial cost functions online, which is critical for applications such as evasion and pursuit. Additionally, it can learn complex, expressive cost functions, parameterized by deep neural networks, eliminating the need for manual design of cost functions typically required in recursive methods (Molloy et al., 2018; Zhao & Molloy, 2024; Self et al., 2020c). While some prior methods have demonstrated good performance with online IOC (Zhao & Molloy, 2024; Molloy et al., 2020; Self et al., 2020c) and deep neural network-based cost functions (Finn et al., 2016a; Fu et al., 2017; Ho & Ermon, 2016; Zeng et al., 2022; Swamy et al., 2021), to the best of our knowledge, no previous approach has successfully combined these two properties.

3 Background

3.1 Maximum Entropy Inverse Reinforcement Learning

Our Inverse reinforcement learning method builds on Guided Cost learning framework Finn et al. (2016b) which is derived from maximum entropy Inverse Reinforcement Learning (IRL) (Ziebart et al., 2008). Our method seeks to learn an expert cost function or rewards function by observing the expert's behavior. The framework assumes the demonstrated expert behavior to be the result of the expert acting stochastically and near-optimally with respect to an unknown cost function. Specifically, the model assumes that the expert samples the demonstrated trajectories τ_i from the distribution (Finn et al., 2016b):

$$p_\theta(\tau) = \frac{1}{\mathcal{Z}_\theta} \exp(-c_\theta(\tau)) \tag{1}$$

where $\tau = \{x_1, u_1, \ldots, x_N, u_N\}$ is a trajectory sample, x_N and u_N are the agent's observed state and control input at time N. $c_\theta(\tau) = \sum_{k=1}^{N} c_\theta(x_k, u_k)$ is the cost function parameterized by $\theta \in \mathcal{W} \subseteq \mathbb{R}^{d_\theta}$, and $\mathcal{Z}_\theta = \int \exp(-c_\theta(\tau))\, d\tau$ is the partition function. Here d_θ denotes the number of parameters and $\mathcal{W}$ is the space of admissible parameters determined by the chosen network architecture (see Section B.2). The parametric family $\{p_\theta\}_{\theta\in\mathcal{W}}$, equivalently $\{c_\theta\}_{\theta\in\mathcal{W}}$, is assumed known and twice-differentiable with respect to θ. That is, the functional form of c_θ is fixed a priori and only the parameters θ are unknown and must be inferred from observed expert behavior.

The partition function $\mathcal{Z}$ is difficult to compute for large or continuous domains, and presents the main computational challenge in maximum entropy IRL. In the sample-based approach to maximum entropy IRL (Finn et al., 2016b; Fu et al., 2017; Ho & Ermon, 2016; Finn et al., 2016a) the partition function $\mathcal{Z}$ is estimated from a background distribution $q(\tau)$ representing the inner control policy, where τ are sampled from the policy $q(\tau)$. The central idea behind the maximum entropy approach is to estimate θ that maximizes the likelihood of the maximum entropy distribution $p_\theta(\tau)$:

$$\hat{\theta} = \arg\max_{\theta} \quad p_\theta(\tau).$$

This approach is equivalent to minimizing the negative log-likelihood of Equation Equation (1) given by Finn et al. (2016b):

$$\mathcal{L}_{\text{IRL}}(\theta) = \frac{1}{N} \sum_{\tau_i \in \mathcal{D}_{\text{demo}}} c_\theta(\tau_i) + \log \mathcal{Z}_\theta \tag{2}$$

Since $\mathcal{Z}_\theta$ is intractable to compute exactly in large or continuous domains, we resort to importance sampling. We introduce a background distribution $q(\tau)$ representing the inner control policy, and rewrite the partition

function by multiplying and dividing the integrand by $q(\tau)$:

$$\mathcal{Z}_\theta = \int \exp(-c_\theta(\tau))\, d\tau = \int \frac{\exp(-c_\theta(\tau))}{q(\tau)}\, q(\tau)\, d\tau = \mathbb{E}_{q(\tau)}\left[\frac{\exp(-c_\theta(\tau))}{q(\tau)}\right]. \tag{3}$$

This expectation is then approximated by drawing M sample trajectories $\{\tau_j\}_{j=1}^M$ from $q(\tau)$:

$$\mathcal{Z}_\theta \approx \frac{1}{M}\sum_{j=1}^{M} \frac{\exp(-c_\theta(\tau_j))}{q(\tau_j)}, \quad \tau_j \sim q(\tau). \tag{4}$$

Substituting equation 4 into equation 2 yields the sample-based negative log-likelihood given by Finn et al. (2016b):

$$\mathcal{L}_{\text{IRL}}(\theta) \approx \frac{1}{N}\sum_{\tau_i \in \mathcal{D}_{\text{demo}}} c_\theta(\tau_i) + \log \frac{1}{M}\sum_{\tau_j \in \mathcal{D}_{\text{samp}}} \frac{\exp(-c_\theta(\tau_j))}{q(\tau_j)} \tag{5}$$

where $\mathcal{D}_{\text{samp}}$ is the set of M background samples drawn from the inner control policy $q(\tau)$, and $\mathcal{D}_{\text{demo}}$ is the set of N expert demonstrations.

To represent the cost function $c_\theta(\tau)$, IOC or IRL feature-based methods typically use a linear combination of hand-crafted features $f : (u, x) \mapsto f(u, x)$, leading to $c_\theta(\tau) = \theta^T f(u_t, x_t)$ (Abbeel & Ng, 2004). This representation is difficult to apply to more complex domains (Finn et al., 2016b). Recent works have focused on the use of high-dimensional expressive function approximators, representing $c_\theta(\tau)$ using neural networks, and outperforming feature-based methods (Finn et al., 2016b; Fu et al., 2017; Ho & Ermon, 2016). In this work, we only leverage neural networks to represent the cost function although, other parameterizations could also be used with our method. In practice, the negative log-likelihood in equation 5 is minimized using gradient descent and batch training. Previous algorithms using deep networks as the cost function parameterization required long and multiple expert demonstrations and sampled trajectories from background policies in order to converge through multiple training iterations. Moreover, training could not proceed before generating all expert and sampled trajectories which restricted it to offline training paradigms. In this work, we introduce a recursive optimization algorithm that adapts network parameters θ on the fly whenever an expert demonstration is observed.

3.2 Kalman Filter as Recursive Second-Order Optimizer

The Kalman Filter (KF) is among the most widely used state estimators in engineering applications. This algorithm recursively estimates the state variables, for example, the position and velocity of a projectile in a noisy linear dynamical system (Lipton et al., 1998), by minimizing the mean-squared estimation error of the current state, as noisy measurements are received and as the system evolves in time (Humpherys et al., 2012). Each update provides the latest unbiased estimate of the system variables. Since the updating process is fairly general and relatively easy to compute, the KF can often be implemented in real-time. When dealing with nonlinear systems extensions of the KF exist such as the EKF which resorts to linearizations using first-order Taylor's expansions Särkkä & Svensson (2023).

Humpherys et al. (2012) showed that the Kalman filter and the EKF, which are recursive algorithms for estimating states in noisy dynamical systems (Lipton et al., 1998; Särkkä & Svensson, 2023), can be derived as special cases of recursive second-order Newton optimization. While this overarching framework can be applied to loss functions beyond MSE, in the classical filtering context it is applied to cumulative MSE loss functions of the form (Humpherys et al., 2012):

$$J_n(X_n, Y_n) = \sum_{k=1}^{n} j_k(x_k, y_k) \tag{6}$$

where $X_n = \{x_1, \ldots, x_n\}$ and x_n represents the state of interest at step n. Moreover, $Y_n = \{y_1, \ldots, y_n\}$ where y_n represents the measurement data at step n. j_k represents the cost at step k associated with x_k and y_k, while J_n is the cumulative value of j_k and represents the cumulative cost associated with sequences X_n and Y_n.

The EKF estimates the state x_n that minimizes equation 6, where j_k is specifically an MSE cost function, at step n using second-order Newton method as new measurement y_n arrives. Thus, equation 6 can be re-written as:

$$J_n(X_n, Y_n) = J_{n-1}(X_{n-1}, Y_{n-1}) + j_n(x_n, y_n) \tag{7}$$

The EKF finds x_n that minimizes equation 7 given previous loss function J_{n-1}, previous state estimates of X_{n-1}, previous measurements Y_{n-1} and current measurement y_n.

To illustrate, consider a nonlinear system $x_k = f_k(x_{k-1}, u_k) + w_k$ with observations $y_k = h_k(x_k) + v_k$, where w_k and v_k are zero-mean noise with covariances Q_k and R_k. The cumulative MSE-EKF loss over the state sequence $X_k = \{x_0, \ldots, x_k\}$ is:

$$J_k(X_k) = \frac{1}{2}\sum_{i=1}^{k}\|y_i - h_i(x_i)\|^2_{R_i^{-1}} + \frac{1}{2}\sum_{i=1}^{k}\|x_i - f_i(x_{i-1}, u_i)\|^2_{Q_i^{-1}} \tag{8}$$

Applying a single Newton step with the judicious initial guess described above yields the EKF updates:

$$P_{k|k-1} = F_k P_{k-1} F_k^\top + Q_k, \quad \hat{x}_{k|k-1} = f_k(\hat{x}_{k-1}, u_k), \tag{9}$$

$$P_k = \left(P_{k|k-1}^{-1} + H_k^\top R_k^{-1} H_k\right)^{-1}, \quad \hat{x}_k = \hat{x}_{k|k-1} - P_k H_k^\top R_k^{-1}(h_k(\hat{x}_{k|k-1}) - y_k) \tag{10}$$

where $F_k = Df_k(\hat{x}_{k-1}, u_k)$ and $H_k = Dh_k(\hat{x}_{k|k-1})$ are the Jacobians, and P_k is the lower-right block of the inverse Hessian (which equals the estimation covariance in the EKF setting).

As shown in Humpherys et al. (2012), when the system dynamics are linear, J_n is a positive-definite quadratic form and a single Newton step yields the exact minimizer regardless of the initial guess. By choosing a judicious initial guess, specifically the minimizer of J_{n-1} extended by one block, the Newton update simplifies to a recursive formula that only requires the previous estimate, the new data, and a matrix P_n that recursively accumulates second-order curvature information. When the dynamics are nonlinear, as in the EKF (Särkkä & Svensson, 2023), the loss is no longer quadratic and a single Newton step yields only an approximation.

In classical Kalman filtering applications such as navigation and target tracking (Ward et al., 2006; Roumeliotis & Bekey, 2000), the goal is to estimate states x_n given sequences of noisy (often Gaussian) data y_n. In our IRL setting, however, we aim at estimating the parameters θ of the cost function $c_\theta(\tau)$ from expert demonstration $\tau \in D_{\text{demo}}$ recursively. To do this, we apply the recursive second order optimization framework to the moment-matching loss derived in Section 4. Unlike the EKF where each x_k is a distinct state that evolves according to system dynamics, θ_k is a single fixed unknown and the sequence $\hat{\theta}_1, \hat{\theta}_2, \ldots$ represents successive estimates refined as more expert demonstrations are observed. The per-step cost j_k becomes the moment-matching term plus a regularization penalty. Since the loss is not MSE, the resulting algorithm is not a Kalman filter but is *akin to* the EKF in that each Newton step yields an approximation of parameters θ.The full derivation is presented in Section 5.

4 Moment Matching as Upper Bound of the Negative Log-likelihood

In this section, we derive an upper-bound of the negative log-likelihood, leading to an optimization problem that is suitable for KF-like online estimation of the parameter vector θ. That is, the resulting upper bound can be written following the same summation structure of equations 6 and 7. The log-sum term in equation 5 prevents direct recursive minimization, but the derived upper bound resolves this issue and enables sequential optimization.

We begin by stating two mild, practically motivated conditions that will be needed to establish the bound.

Condition 1 (Bounded Non-negative Cost Function). The cost function $c_\theta(\tau)$ is constrained to take bounded values, i.e., there exists a constant $-\infty < c_{\min} < c_{\max} < \infty$ such that:

$$c_{\min} \leq c_\theta(\tau) \leq c_{\max}, \quad \forall\, \theta \in \mathcal{W},\ \forall\, \tau. \tag{11}$$

This is achievable through standard architectural choices, such as a ReLU activation with output clipping, or a sigmoid output layer.

Condition 2 (Bounded Sampling Density). The sampling density $q(\tau)$ is constrained to take non-zero bounded values.

This is achievable through control policy choice such as MPPI. The MPPI sampling distribution $q(\tau)$ operates over a compact control space $\mathcal{U} = [u_{\min}, u_{\max}]$ (reflecting physical actuator limits) with its mean μ constrained to $\mathcal{U}$. Since MPPI samples controls from a Gaussian $\mathcal{N}(\mu, \Sigma)$ with $\mu \in \mathcal{U}$, the density evaluated at any $u \in \mathcal{U}$ is bounded:

$$0 < q_{\min} \leq q(\tau) \leq q_{\max} < \infty, \quad \forall\, \tau \in \mathcal{U}, \tag{12}$$

where

$$q_{\max} = (2\pi)^{-d/2}|\Sigma|^{-1/2}, \tag{13}$$

$$q_{\min} = (2\pi)^{-d/2}|\Sigma|^{-1/2} \exp\left(-\tfrac{1}{2}D_{\max}\right), \tag{14}$$

with $D_{\max} = \max_{u\in\mathcal{U},\, \mu\in\mathcal{U}}(u-\mu)^\top\Sigma^{-1}(u-\mu)$ being a finite constant determined by $\mathcal{U}$ and Σ. Since both μ and u are constrained to the compact set $\mathcal{U}$ and Σ is fixed, both $q_{\min}$ and $q_{\max}$ are finite positive constants determined entirely by algorithmic design parameters ($\mathcal{U}$, Σ), independent of θ.

In Matkovic & Pecaric (2007), the authors present a Jensen's reversed inequality for convex functions as follows. Let $[a, b]$ be an interval in $\mathbb{R}$, $y_1, \ldots, y_N \in [a, b]$, and $p_1, \ldots, p_N$ be positive real numbers such that $\sum_{n=1}^{N} p_n = 1$. If $f : [a, b] \to \mathbb{R}$ is convex on $[a, b]$, then (Corollaries 3 and 4) of Matkovic & Pecaric, 2007) :

$$\sum_{n=1}^{N} p_n f(y_n) - f\left(\sum_{n=1}^{N} p_n y_n\right) \leq \quad f(a) + f(b) - 2f\left(\frac{a+b}{2}\right) \tag{15}$$

Replacing the function f by the negative log function, $f = -\log$ which is a convex function on $]0, \infty[$, equation 15 can be re-written as Matkovic & Pecaric (2007) :

$$\log\left(\sum_{n=1}^{N} p_n y_n\right) \leq \sum_{n=1}^{N} p_n \log(y_n) - \log(a) - \log(b) + 2\log\left(\frac{a+b}{2}\right) \tag{16}$$

We apply equation 16 to the log-sum term in the sample-based negative log-likelihood equation 5. We define:

$$p_j = \frac{1}{M} \quad \text{and} \quad y_j = \frac{\exp(-c_\theta(\tau_j^{\text{samp}}))}{q(\tau_j^{\text{samp}})}, \quad j = 1, \ldots, M, \tag{17}$$

where τ_j^{samp} is a trajectory sampled from $\mathcal{D}_{\text{samp}}$.

Lemma 4.1 (Bounds on y_j)**.** *Under Conditions 1 and 2, the quantities y_j defined in equation 17 satisfy $y_j \in [a, b]$ where:*

$$a = \frac{\exp(-c_{\max})}{q_{\max}} > 0, \qquad b = \frac{\exp(-c_{\min})}{q_{\min}} < \infty. \tag{18}$$

Both a and b are positive, finite constants that depend only on architectural and algorithmic design parameters, and are independent of θ.

Proof. Since $c_{\min} \leq c_\theta(\tau) \leq c_{\max}$, we have $\exp(-c_{\max}) \leq \exp(-c_\theta(\tau)) \leq \exp(-c_{\min})$. Combined with $0 < q_{\min} \leq q(\tau) \leq q_{\max}$, we obtain:

$$\frac{\exp(-c_{\max})}{q_{\max}} \leq \frac{\exp(-c_\theta(\tau))}{q(\tau)} \leq \frac{\exp(-c_{\min})}{q_{\min}}. \tag{19}$$

Note that $a > 0$ follows from the exponential structure of the maximum entropy distribution: since $\exp(-x) > 0$ for all finite $x \in \mathbb{R}$, finiteness of $c_{\max}$ guarantees $\exp(-c_{\max}) > 0$, and thus $a > 0$. □

By Lemma 4.1, the requirements of the reverse Jensen's inequality equation 16 are satisfied. Substituting equation 17 into equation 16, we obtain an upper bound on the log-sum term:

$$\log \frac{1}{M} \sum_{j=1}^{M} \frac{\exp(-c_\theta(\tau_j^{\text{samp}}))}{q(\tau_j^{\text{samp}})} \leq \frac{1}{M} \sum_{j=1}^{M} \left(-c_\theta(\tau_j^{\text{samp}}) - \log q(\tau_j^{\text{samp}})\right) - K, \tag{20}$$

where

$$K = \log(a) + \log(b) - 2\log\left(\frac{a+b}{2}\right), \tag{21}$$

which depends only on $c_{\max}$, $q_{\min}$, and $q_{\max}$, all fixed by the network architecture and MPPI configuration. Therefore, K is independent of θ.

Replacing equation 20 in the sample-based negative log-likelihood equation 5, we derive the following upper bound:

$$\begin{aligned} \mathcal{L}_{\text{IRL}}(\theta) &= \frac{1}{N} \sum_{i=1}^{N} c_\theta(\tau_i^{\text{demo}}) + \log \frac{1}{M} \sum_{j=1}^{M} \frac{\exp(-c_\theta(\tau_j^{\text{samp}}))}{q(\tau_j^{\text{samp}})} \\ &\leq \frac{1}{N} \sum_{i=1}^{N} c_\theta(\tau_i^{\text{demo}}) + \frac{1}{M} \sum_{j=1}^{M} \left(-c_\theta(\tau_j^{\text{samp}}) - \log q(\tau_j^{\text{samp}})\right) - K. \end{aligned} \tag{22}$$

Since $\log q(\tau_j^{\text{samp}})$ and K are independent of θ—noting that in practice $q(\tau)$ is determined by the cost function parameters from the previous optimization iteration, which are held fixed during the current update—minimizing this upper bound over θ is equivalent to minimizing:

$$\mathcal{L}_{\text{UB-MM}} = \frac{1}{N} \sum_{i=1}^{N} c_\theta(\tau_i^{\text{demo}}) - \frac{1}{M} \sum_{j=1}^{M} c_\theta(\tau_j^{\text{samp}}). \tag{23}$$

By multiplying and dividing the second term by N and partitioning the M background samples into N groups of M/N samples each (one group per expert demonstration), we can factor out $\frac{1}{N}$ and rewrite equation 23 as:

$$\mathcal{L}_{\text{UB-MM}} = \frac{1}{N} \sum_{i=1}^{N} \left[c_\theta(\tau_i^{\text{demo}}) - \frac{N}{M} \sum_{k=1}^{M/N} c_\theta(\tau_{i,k}^{\text{samp}}) \right], \tag{24}$$

where $\tau_{i,k}^{\text{samp}}$ denotes the k-th background sample associated with the i-th expert demonstration. This form makes explicit that each expert demonstration is paired with M/N background samples, with $M \geq N$.

For compactness and computational efficiency in the recursive setting, we set $M = N$, i.e., for each expert demonstration we draw one sampled trajectory from the inner control policy $q(\tau)$. Under this choice, the factor $N/M = 1$ and the inner sum in equation 24 collapses to a single term, yielding:

$$\mathcal{L}_{\text{UB-MM}} = \frac{1}{N} \sum_{i=1}^{N} \left[c_\theta(\tau_i^{\text{demo}}) - c_\theta(\tau_i^{\text{samp}}) \right]. \tag{25}$$

This upper bound has a particularly important consequence: it transforms the maximum entropy IRL objective into a moment-matching loss. This structure is equivalent to recent moment matching formulations in IRL (Swamy et al., 2021; Zeng et al., 2022; 2025), which replace the log-partition function of MaxEnt IRL with expectation-matching objectives between expert and policy distributions. Our derivation shows that moment matching losses, particularly the formulation in Swamy et al. (2021), can be interpreted as an upper bound of the maximum entropy negative log-likelihood.

Remark 4.2 (Tightness of the bound). The tightness of the upper bound equation 22 depends on the choice of cost function parameterization and sampling policy. In our experimental settings the bound remains effective, as demonstrated by the empirical results in Section 6.

5 Recursive Deep Inverse Reinforcement Learning

In the previous section, we derived the upper bound of the negative log-likelihood cost described in equation 5 and showed it's equivalent to moment matching (Swamy et al., 2021). In this section, we seek to minimize the moment matching loss of equation 25 recursively. To do so, we re-write the EKF optimization problem using the loss function derived in equation 25 and a regularization term.

We exploit this structure by applying a single optimization step per iteration, analogous to the EKF. At step i, the algorithm predicts $\hat{\theta}_{i|i-1} = \hat{\theta}_{i-1}$, then updates this prediction using the gradient of the new moment-matching term, scaled by a matrix P_{θ_i} that recursively accumulates curvature information and acts as an adaptive step size. The result is a fully online algorithm: one expert trajectory in, one parameter update out, with no storage of past data. We first describe the optimization formulation and define all relevant quantities, then derive the recursive solution.

5.1 Problem Formulation

Given an expert trajectory $\mathcal{D}_{\text{demo}} \triangleq \{\tau^{(0)}, \ldots, \tau^{(N-1)}\}$ we seek to determine an optimal solution θ_i^* starting from initial condition θ_0 by solving the following mathematical optimization problem:

$$\begin{aligned}\mathcal{L}_N(\Theta_N) &= \mathcal{L}_{\text{UB-MM}} + \frac{1}{2}\sum_{i=1}^{N}\|\theta_i - \theta_{i-1}\|^2_{Q_\theta^{-1}} \\ &= \sum_{i=1}^{N}\left[c_\theta(\tau_i^{\text{demo}}) - c_\theta(\tau_i^{\text{samp}})\right] + \frac{1}{2}\sum_{i=1}^{N}\|\theta_i - \theta_{i-1}\|^2_{Q_\theta^{-1}},\end{aligned} \tag{26}$$

where $\Theta_N = \{\theta_0, \ldots, \theta_N\}$ denotes the full sequence of parameter estimates. The second term penalizes large changes in θ between consecutive optimization steps, acting as a regularization controlled by $Q_\theta \in \mathbb{R}^{d_\theta \times d_\theta}$ (Imbiriba et al., 2022; Ghanem et al., 2025). The notation $\|x\|^2_{Q_\theta^{-1}} = x^\top Q_\theta^{-1} x$ denotes the energy norm with respect to Q_θ^{-1}.

Before stating the recursive solution, we define all quantities used in the algorithm. Let $\Theta_i = \{\theta_0, \ldots, \theta_i\}$ denote the full sequence of parameter estimates up to step i, and let $\hat{\Theta}_{i-1}$ denote the optimized sequence from the previous step. Let $\hat{\theta}_i$ denote the parameter estimate at step i, and let $\hat{\theta}_{i|i-1} = \hat{\theta}_{i-1}$ denote the parameter estimate before incorporating the new expert sample at step i. The predicted sequence is:

$$\hat{\Theta}_{i|i-1} = \begin{bmatrix}\hat{\Theta}_{i-1} \\ \hat{\theta}_{i|i-1}\end{bmatrix}, \tag{27}$$

which extends the previous sequence by repeating the last estimate.

Let $\mathcal{L}_i(\Theta_i)$ denote the cumulative loss at step i as defined in equation 26. We define the following gradient and Hessian quantities of the cost function, evaluated at $\hat{\theta}_{i-1}$:

$$C_{\tau_{\text{demo}}}(i) = \frac{\partial c_\theta(\tau_i^{\text{demo}})}{\partial \hat{\theta}_{i-1}}, \qquad C_{\tau_{\text{samp}}}(i) = \frac{\partial c_\theta(\tau_i^{\text{samp}})}{\partial \hat{\theta}_{i-1}}, \tag{28}$$

$$C^2_{\tau_{\text{demo}}}(i) = \frac{\partial^2 c_\theta(\tau_i^{\text{demo}})}{\partial^2 \hat{\theta}_{i-1}}, \qquad C^2_{\tau_{\text{samp}}}(i) = \frac{\partial^2 c_\theta(\tau_i^{\text{samp}})}{\partial^2 \hat{\theta}_{i-1}}. \tag{29}$$

Additionally, we define:

- $P_{\theta_i} \in \mathbb{R}^{d_\theta \times d_\theta}$: the lower-right block of the full inverse Hessian $\left(\nabla^2 \mathcal{L}_i(\hat{\Theta}_{i|i-1})\right)^{-1}$, representing accumulated second-order curvature information and acting as an adaptive step-size matrix; initialized as $P_{\theta_0} = 10^{-2} I$.
- $Q_\theta \in \mathbb{R}^{d_\theta \times d_\theta}$: the regularization matrix, initialized as $Q_\theta = 10^{-4} I$, which prevents P_{θ_i} from collapsing to zero and keeps the algorithm responsive to new data.

5.2 Derivation of the Recursive Solution

Inspired by the recursive second-order optimization framework described in Humpherys et al. (2012), we seek to determine the optimal solution $\Theta_N^* = \{\theta_0^*, \ldots, \theta_N^*\}$ using the second-order Newton method sequentially, which recursively finds Θ_N^* given Θ_{N-1}^*.

At each step i, RDIRL minimizes the cumulative loss $\mathcal{L}_i(\Theta_i)$ over the full sequence $\Theta_i = \{\theta_0, \ldots, \theta_i\}$ by performing one Newton step. Because the loss has the recursive structure of equation 26, this Newton step can be computed using only $\hat{\Theta}_{i-1}$ and the new pair $(\tau_i^{\text{demo}}, \tau_i^{\text{samp}})$, without revisiting past data. Of the updated sequence $\hat{\Theta}_i$, only the last block $\hat{\theta}_i$ is retained as the new parameter estimate; earlier blocks remain unchanged from $\hat{\Theta}_{i-1}$. The matrix P_{θ_i} accumulates second-order curvature information and acts as an adaptive step size.

We start by breaking the optimization function equation 26 as follows:

$$\mathcal{L}_i(\Theta_i) = \mathcal{L}_{i-1}(\Theta_{i-1}) + c_\theta(\tau_i^{\text{demo}}) - c_\theta(\tau_i^{\text{samp}}) + \frac{1}{2}\|\theta_i - \theta_{i-1}\|^2_{Q_\theta^{-1}}. \tag{30}$$

Next, we further divide equation 30 into a prediction step and an update step:

$$\mathcal{L}_i(\Theta_i) = \mathcal{L}_{i|i-1}(\Theta_i) + c_\theta(\tau_i^{\text{demo}}) - c_\theta(\tau_i^{\text{samp}}), \tag{31}$$

where

$$\mathcal{L}_{i|i-1}(\Theta_i) = \mathcal{L}_{i-1}(\Theta_{i-1}) + \frac{1}{2}\|\theta_i - \theta_{i-1}\|^2_{Q_\theta^{-1}}. \tag{32}$$

Our optimization approach consists of first minimizing equation 32 to obtain the predictor $\hat{\Theta}_{i|i-1}$, then minimizing equation 31 given this predictor. We minimize equation 32 with respect to Θ_i by finding Θ_i that drives the gradient to zero. Taking the gradient of equation 32 with respect to Θ_i, we obtain:

$$\nabla\mathcal{L}_{i|i-1}(\Theta_i) = \begin{bmatrix} \nabla\mathcal{L}_{i-1}(\Theta_i) - L_\theta^T Q_\theta^{-1}[\theta_i - \theta_{i-1}] \\ Q_\theta^{-1}[\theta_i - \theta_{i-1}] \end{bmatrix} \tag{33}$$

with $L_\theta = [0_{d_\theta \times d_\theta}, \ldots, 0_{d_\theta \times d_\theta}, I_{d_\theta \times d_\theta}]$ where $L_\theta \in \mathbb{R}^{d_\theta \times ((i-1)\times d_\theta)}$.

Setting $\nabla\mathcal{L}_{i|i-1}(\Theta_i) = 0$, the minimizer $\hat{\Theta}_{i|i-1}$ can be decomposed as:

$$\hat{\Theta}_{i|i-1} = \begin{bmatrix} \hat{\Theta}_{i-1} \\ \hat{\theta}_{i-1} \end{bmatrix}. \tag{34}$$

Given equation 34, we proceed to minimize equation 31 using the second-order Newton update. The gradient of equation 31 at $\Theta_i = \hat{\Theta}_{i|i-1}$ is:

$$\nabla\mathcal{L}_i(\Theta_i) = \begin{bmatrix} \mathbf{0}_{(i-1)\cdot d_\theta} \\ C_{\tau_{\text{demo}}}(i) - C_{\tau_{\text{samp}}}(i) \end{bmatrix} \tag{35}$$

and the Hessian of equation 31 is:

$$\nabla^2\mathcal{L}_i(\Theta_i) = \begin{bmatrix} \nabla^2\mathcal{L}_{i-1}(\Theta_{i-1}) + Q_\theta^{-1} & -L_\theta^T Q_\theta^{-1} \\ -Q_\theta^{-1} L_\theta & Q_\theta^{-1} + C^2_{\tau_{\text{demo}}}(i) - C^2_{\tau_{\text{samp}}}(i) \end{bmatrix}. \tag{36}$$

Using the Newton second-order method, we update our estimate of Θ_i given $\hat{\Theta}_{i|i-1}$ as follows:

$$\hat{\Theta}_i = \hat{\Theta}_{i|i-1} - \left(\nabla^2\mathcal{L}_i(\hat{\Theta}_{i|i-1})\right)^{-1} \nabla\mathcal{L}_i(\hat{\Theta}_{i|i-1}). \tag{37}$$

The resulting optimal variable $\hat{\theta}_i \in \hat{\Theta}_i$ is obtained by extracting the last d_θ-dimensional block of equation 37, which leads to the following theorem.

Theorem 5.1. *Given $\hat{\theta}_{i-1} \in \hat{\Theta}_{i-1}$ and known $P_{\theta_{i-1}} \in \mathbb{R}^{d_\theta \times d_\theta}$, the recursive equations for computing $\hat{\theta}_i$ that minimizes equation 31 are given by the following:*

$$\hat{\theta}_i = \hat{\theta}_{i|i-1} - P_{\theta_i}(C_{\tau_{\text{demo}}}(i) - C_{\tau_{\text{samp}}}(i)) \tag{38}$$

where $\hat{\theta}_{i|i-1} = \hat{\theta}_{i-1}$ is the predicted parameter. P_{θ_i} being the lower right block of $\left(\nabla^2 \mathcal{L}_i(\hat{\Theta}_{i|i-1})\right)^{-1}$ recursively calculated as:

$$P_{\theta_i} = \left[(P_{\theta_{i-1}} + Q_\theta)^{-1} + \left(C^2_{\tau_{\text{demo}}}(t_i) - C^2_{\tau_{\text{samp}}}(t_i)\right)\right]^{-1} \tag{39}$$

Proof. By the Schur complement formula (block matrix inversion lemma) applied to the Hessian equation 36, the lower-right block of $\left(\nabla^2 \mathcal{L}_i(\hat{\Theta}_{i|i-1})\right)^{-1}$ is:

$$P_{\theta_i} = \left[\left(P_{\theta_{i-1}} + Q_\theta\right)^{-1} + C^2_{\tau_{\text{demo}}}(i) - C^2_{\tau_{\text{samp}}}(i)\right]^{-1}, \tag{40}$$

where $P_{\theta_{i-1}} = \left(\nabla^2 \mathcal{L}_{i-1}\right)^{-1}_{\theta\theta}$ is the lower-right block of the previous inverse Hessian, and the term $(P_{\theta_{i-1}} + Q_\theta)^{-1}$ arises from the regularization term in equation 32. This derivation applies Lemma B.3 of Humpherys et al. (2012). Substituting this into the last d_θ rows of the Newton update equation 37, together with the gradient equation 35, yields equation 38. □

As a consequence of Theorem 5.1, $\hat{\theta}_i$ is computed according to equation 38 using only $\hat{\theta}_{i-1}$, the new trajectories $(\tau_i^{\text{demo}}, \tau_i^{\text{samp}})$, and the accumulated inverse Hessian $P_{\theta_{i-1}}$. The entire training procedure is detailed in Algorithm 1.

5.3 Algorithm Description

Algorithm 1 maintains a cost function $c_\theta(\tau)$ parameterized by θ, which maps trajectories τ to scalar costs. The goal is to iteratively update θ such that trajectories generated from the current policy $q(\tau)$ match the expert demonstrations.

At each outer iteration (episode), we initialize the sampling policy $q(\tau)$, which can be any stochastic policy optimized with methods like PPO or MPPI. We also initialize the inverse Hessian P_{θ_0} and the regularization matrix Q_θ. The matrix P_{θ_0} represents the initial step-size scaling for the Newton updates, and Q_θ controls the regularization strength, preventing P_{θ_i} from collapsing to zero across iterations.

For each inner iteration, as soon as the algorithm observes one expert demonstration τ_i^{demo}, it samples a trajectory τ_i^{samp} from $q(\tau)$. The gradients $C_{\tau_{\text{demo}}}(i)$ and $C_{\tau_{\text{samp}}}(i)$, as well as the Hessians $C^2_{\tau_{\text{demo}}}(i)$ and $C^2_{\tau_{\text{samp}}}(i)$, are then computed. The parameter θ is updated via equation 38 and the inverse Hessian via equation 39. After updating θ, the sampling policy $q(\tau)$ is improved using any standard policy optimization method (e.g., PPO, MPPI), guided by the updated cost function c_θ. This process continues over K episodes, gradually aligning the agent's behavior with that of the expert.

6 Experiments

We evaluate the proposed RDIRL algorithm in continuous control benchmarks from OpenAI Gym (Brockman, 2016) and MuJoCo (Todorov et al., 2012), as well as in an adversarial cognitive radar scenario (Potter et al., 2024; Haykin, 2006). We compare its performance against state-of-the-art inverse reinforcement learning and imitation learning methods, including Generative Adversarial Imitation Learning (GAIL) (Ho & Ermon, 2016), Guided Cost Learning (GCL) (Finn et al., 2016b), Adversarial Inverse Reinforcement Learning (AIRL) (Fu et al., 2017), SQIL (Reddy et al., 2020), and Maximum Likelihood Inverse Reinforcement Learning (ML-IRL) (Zeng et al., 2022), a moment-matching variant of IRL. Experiments are conducted in two regimes: batch mode (section 6), where competing methods are trained in their standard setting with full trajectory batches, and streaming mode, where updates occur sample by sample (Appendix B.3).

Algorithm 1: Recursive Deep Inverse Reinforcement Learning

Input: Cost function c_θ with randomly initialized parameters θ_0, regularization matrix Q_θ, initial step-size matrix P_{θ_0}, number of episodes K, number of expert samples per episode N

while episodes $< K$ **do**
  Initialize inner policy $q(\tau)$;
  for $i = 1, 2, \ldots, N$ **do**
    Observe one expert sample τ_i^{demo};
    Sample one trajectory τ_i^{samp} from $q(\tau)$;
    Evaluate the gradients $C_{\tau_{\text{demo}}}(i)$ and $C_{\tau_{\text{samp}}}(i)$;
    Evaluate the Hessians $C^2_{\tau_{\text{demo}}}(i)$ and $C^2_{\tau_{\text{samp}}}(i)$;
    $P_{\theta_i} \leftarrow \left[(P_{\theta_{i-1}} + Q_\theta)^{-1} + C^2_{\tau_{\text{demo}}}(i) - C^2_{\tau_{\text{samp}}}(i)\right]^{-1}$;
    $\hat{\theta}_i \leftarrow \hat{\theta}_{i-1} - P_{\theta_i}\left(C_{\tau_{\text{demo}}}(i) - C_{\tau_{\text{samp}}}(i)\right)$;
    Update $q(\tau)$ w.r.t. c_θ using any policy optimization method;
  episodes $\leftarrow$ episodes $+ 1$;

Unlike reinforcement learning methods such as SAC (Haarnoja et al., 2018) or PPO (Schulman et al., 2017), which require large trajectory batches to converge and thus fail in streaming or real-time settings, our approach leverages MPPI (Williams et al., 2016) as the inner control policy. Since MPPI updates its actions at every time step, it is naturally suited for online IRL. In preliminary experiments, MPPI also provided stable performance and fast convergence unlike traditional RL policies when integrated into the RDIRL framework. Furthermore, preliminary experiments showed that competing IRL methods paired with their original RL inner policies failed to converge in streaming mode too. For consistency and fairness, we therefore adapt all competing methods to use MPPI as the inner policy in both batch and streaming comparisons.

Our results show that RDIRL consistently outperforms all benchmarked methods in recovering reward functions. Policies trained with rewards learned by RDIRL achieve optimal or near-optimal behavior significantly faster than competing approaches. Crucially, unlike existing methods which require large batches of expert trajectories and environment rollouts to converge, RDIRL leverages online adaptation. This enables efficient learning from streaming demonstrations, making it particularly well-suited for adversarial and time-limited scenarios.

Table 1: Comparison of normalized averaged reward values across all episodes for different Gym environments and methods.

Methods	CartPole	MountainCar	HalfCheetah-v4	Hopper
SQIL	0.947 ± 0.088	$-0.001 \pm 4.79 \times 10^{-5}$	-1.56 ± 0.89	0.799 ± 0.15
GAIL	0.934 ± 0.058	0.236 ± 0.203	-0.521 ± 1.15	0.714 ± 0.08
GCL	0.92 ± 0.09	0.247 ± 0.19	-0.226 ± 1.27	0.69 ± 0.075
AIRL	0.953 ± 0.069	0.233 ± 0.204	-0.54 ± 1.11	0.709 ± 0.084
ML-IRL	0.938 ± 0.093	0.253 ± 0.19	-0.32 ± 1.12	0.648 ± 0.06
RDIRL (ours)	$\mathbf{0.993 \pm 0.013}$	$\mathbf{0.68 \pm 0.32}$	$\mathbf{0.496 \pm 0.59}$	$\mathbf{0.803 \pm 0.11}$

6.1 Continuous control

To assess the performance of our proposed approach RDIRL, we conduct inverse reinforcement learning (IRL) experiments on the CartPole and Mountain Car environments from OpenAI Gym (Brockman, 2016) and HalfCheetah-v4, Hopper, and Walker2d from MuJoCo (Todorov et al., 2012), all solved using model-free reinforcement learning. Each task has a predefined true reward function provided by OpenAI Gym.

We first generate expert demonstrations for these tasks by training a PPO reinforcement learning agent (Schulman et al., 2017) to maximize the true reward function. Each expert demonstration consists of a state

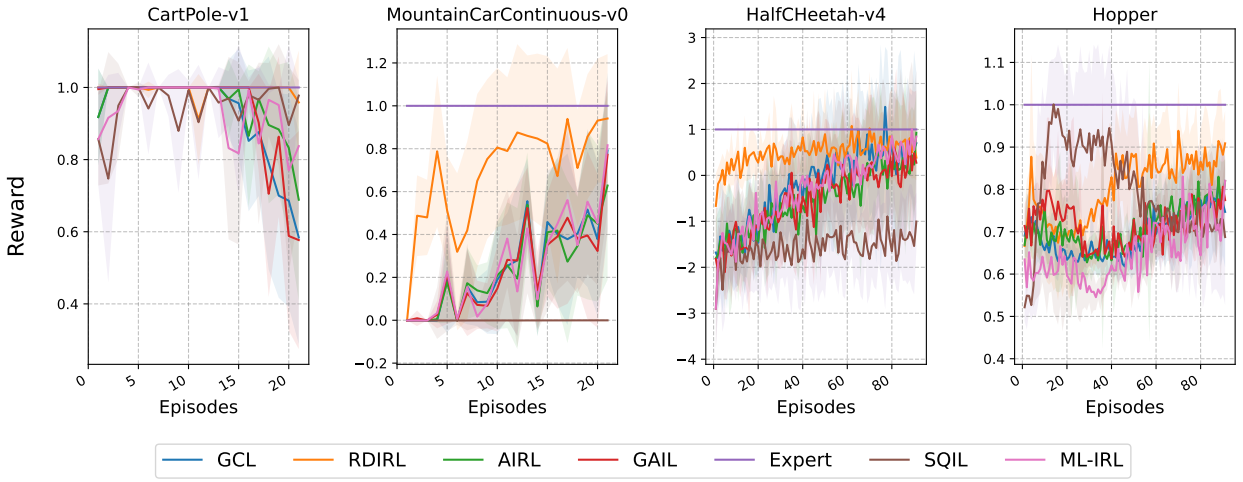

Figure 1: Learning curves for RDIRL and other methods.

trajectory of size N steps specified in Table 3 in B.1 for each task, which is then used as the sole expert trajectory for each IRL algorithm. Note that we only use the expert's state trajectory and not the expert's actions, since we do not have access to the expert's control policy.

Next, we execute RDIRL to learn the reward function and train competing IRL algorithms using the expert trajectory over multiple episodes in batch mode, where each episode consists of an expert trajectory. This process is repeated for 12 Monte Carlo runs with different seeds. In all experiments, we use MPPI as the internal control policy $q(\tau)$ to maximize the learned reward function, $-c_\theta$. A detailed experiment description and parameter values of MPPI and IRL algorithms is described in Appendix B.1

We plot the mean of the normalized cumulative reward values across all episodes of trajectories τ^{samp} sampled from the inner control policy $q(\tau)$ in Figure 1.the averaged reward values are normalized with respect to the expert reward. In the case of RDIRL, τ^{samp} used to calculate the reward function in Figure 1 are generated online during training according to Algorithm 1. For the rest of the methods, τ^{samp} are generated offline after each offline training episode is completed.

All methods use the same neural network architecture to parameterize the reward function. Networks are randomly initialized at the start of each experiment, and all experiments are run on Nvidia-H200 GPU Cluster with 1 GPU per job(seed).

Our proposed method, RDIRL, successfully learns reward functions across all benchmark environments and consistently outperforms competing methods. In CartPole and MountainCar, it quickly recovers the expert reward even converging in one episode in CartPole, while in HalfCheetah and Hopper it achieves faster convergence and higher reward quality than baselines, many of which require far more episodes to converge or fail to converge. Learning curves in Figures 1 and 2 illustrate these improvements, with Walker2d results consistent with Figure 3 in Reddy et al. (2020), where rewards closer to the expert indicate better performance. Furthermore, experimental results in streaming settings with detailed descriptions are provided in Appendix B.3.

Table 1 further shows that RDIRL achieves the highest normalized rewards in most tasks. This consistent outperformance stems from its recursive structure and adaptive uncertainty-aware updates, which improve sample efficiency and stability. Unlike traditional IRL, our method requires no fixed learning rate, as P_θ is updated at each step and acts as an adaptive rate.

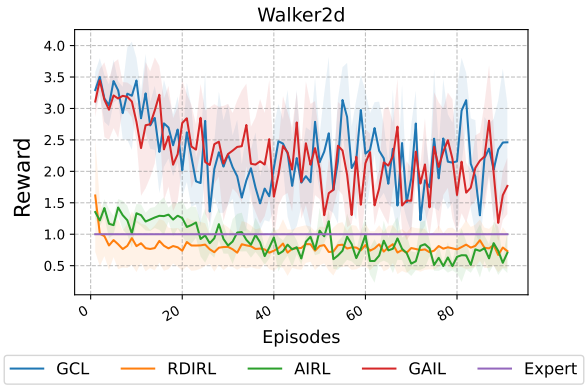

Figure 2: Learning curves for for Walker2d.

6.2 Cognitive radar

To evaluate whether our method can learn cost functions of adversarial agents, we perform inverse reinforcement learning experiments on a cognitive radar task following the setup of Potter et al. (2024). The task involves a radar chasing a moving target in 3D space.

Expert (Radar) Dynamics and Reward. The radar follows the second-order unicycle model of Potter et al. (2024), with state $\chi_k^R = [x, y, z, \theta, v, \omega]$ representing 3D Cartesian position, heading angle θ, heading velocity v, and angular velocity ω. The discrete-time kinematic model is:

$$\chi_{k+1}^R = \chi_k^R + G_k(\chi_k^R, u_k), \tag{41}$$

where

$$G_k(\chi_k^R, u_k) = \begin{bmatrix} v_k \cos(\theta_k) \\ v_k \sin(\theta_k) \\ 0 \\ \omega_k \\ u_a \\ u_{\dot{\omega}} \end{bmatrix} \Delta t, \tag{42}$$

with control inputs $u = [u_a, u_{\dot{\omega}}]^\top$ (linear and angular acceleration) subject to the constraints $\underline{u}_a \leq u_{a_k} \leq \bar{u}_a$ and $\underline{u}_{\dot{\omega}} \leq u_{\dot{\omega}_k} \leq \bar{u}_{\dot{\omega}}$ for all k, and $\Delta t = 0.1$ s is the control timestep. We denote the 3D position components of the radar and target states as $\chi_{xyz}^R = [x, y, z]^\top$ and $\chi_{xyz}^T = [x, y, z]^\top$, respectively.

The radar's true reward function is the log-determinant of the Standard Fisher Information Matrix (FIM) (Potter et al., 2024) for target localization:

$$r = \log\det J(\chi_{xyz}^T;\, \chi_{xyz}^R), \tag{43}$$

where the FIM for a single radar-target pair is given by Potter et al. (2024):

$$J(\chi_{xyz}^T; \chi_{xyz}^R) = (\chi_{xyz}^T - \chi_{xyz}^R)(\chi_{xyz}^T - \chi_{xyz}^R)^\top \left(\frac{4}{\Gamma \|\chi_{xyz}^R - \chi_{xyz}^T\|^6} + \frac{8}{\|\chi_{xyz}^R - \chi_{xyz}^T\|^4} \right), \tag{44}$$

with $\Gamma = \frac{\sigma_a^2 \pi L}{2 P_t \Lambda_t \Lambda_r \Xi}$ determined by the radar signal parameters: transmit power $P_t = 1000$ W, transmit and receive gains $\Lambda_t = \Lambda_r = 200$, radar cross section $\Xi = 1$ m^2, loss factor $L = 1$, carrier frequency $f_c = 10^8$ Hz, and noise power σ_a^2 set such that SNR $= -20$ dB at range $R = 500$ m. The radar expert policy is an MPPI controller that maximizes this FIM reward with horizon $H = 10$, number of sampled trajectories $= 25$, and temperature $= 10^{-2}$.

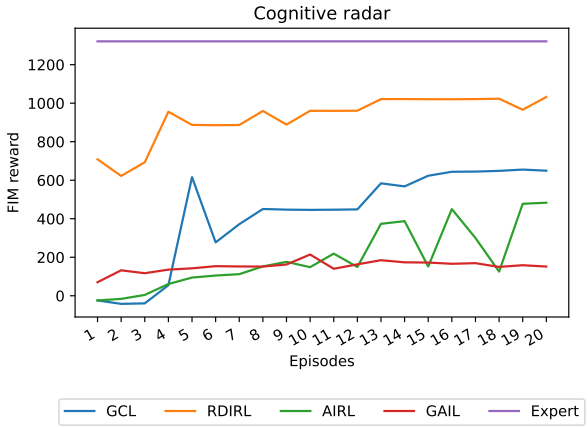

Figure 3: Learning curves for RDIRL and other methods.

Target Dynamics and Learned Reward. The target follows a constant velocity motion model with acceleration noise (Baisa, 2020; Potter et al., 2024), with state $\chi_k^T = [x, y, z, \dot{x}, \dot{y}, \dot{z}]$ and transition model:

$$\chi_{k+1}^T = A_{\text{single}}\, \chi_k^T + \epsilon_w, \quad A_{\text{single}} = \begin{bmatrix} \mathbf{I}_{3\times3} & \Delta t\, \mathbf{I}_{3\times3} \\ \mathbf{0}_{3\times3} & \mathbf{I}_{3\times3} \end{bmatrix}, \tag{45}$$

where $\epsilon_w \sim \mathcal{N}(0, W_{\text{single}})$ with $W_{\text{single}} = W_{\Delta t}\, \Sigma_w\, W_{\Delta t}^\top$, $W_{\Delta t} = \begin{bmatrix} \frac{1}{2}\Delta t^2\, \mathbf{I}_{3\times3} \\ \Delta t\, \mathbf{I}_{3\times3} \end{bmatrix}$, $\Sigma_w = \sigma_W^2\, \mathbf{I}_{3\times3}$, and $\sigma_W = \sqrt{10}$.

The target's goal is to learn the radar's FIM reward function online using RDIRL. The learned cost function c_θ is parameterized by a one-hidden-layer MLP with 128 units and ReLU activation, taking as input the relative displacement $\Delta p = \chi_{xyz}^R - \chi_{xyz}^T \in \mathbb{R}^3$ between the radar and target 3D positions. The output of the network is passed through a ReLU activation to ensure non-negative cost values.

To achieve this goal, we execute Algorithm 1 where the learned cost function approximating the radar's reward is updated online. The inner control policy $q(\tau)$ is an MPPI that maximizes the learned reward function, $-c_\theta$. Additional environment and IRL method's parameters are described in Table 3. Furthermore, we compare

Table 2: Comparison of mean FIM reward values for the Cognitive Radar example obtained by the different IRL methods.

Methods	Mean Cumulative Reward
GAIL	153.05
GCL	423.49
AIRL	196.53
RDIRL (ours)	**924.78**

RDIRL against GAIL, AIRL, and GCL. To implement these methods, we generate expert trajectories for multiple episodes, where the expert policy is an MPPI that maximizes the radar's FIM. The inner control policy $q(\tau)$ in all of these baselines is an MPPI, with parameters specified in Table 3. We repeat this process for 5 Monte Carlo runs using different seeds. To test if the target successfully learned the radar's reward function, we execute the radar using an MPPI policy that maximizes the learned reward function $-c_\theta$ instead of the true FIM. We plot the cumulative true FIM values resulting from the trajectories τ^{samp} sampled from the inner control policy $q(\tau)$ in Figure 3. We compare RDIRL's performance in learning the radar's reward function against GAIL, GCL, and AIRL. In the case of RDIRL, τ^{samp} used to evaluate the learned reward function in Figure 3 are generated online during training according to Algorithm 1. For the rest of the methods, τ^{samp} are generated offline after each offline training episode is completed. In all algorithms, we

used the same neural network architecture described above to parameterize the learned reward function: one hidden layer of 128 units, with a ReLU activation function. All networks were always initialized randomly at the start of each experiment and all experiments are run on an Intel Core i7 CPU.

Results in Figure 3 show that RDIRL successfully learns the radar's FIM with a much faster convergence rate than the benchmark methods. The mean cumulative reward values across all episodes for each method are summarized in Table 2. As shown, RDIRL outperforms all other methods in terms of the mean cumulative reward, significantly outperforming the benchmark methods (i.e., AIRL, GCL, and GAIL).

7 Conclusions

We presented RDIRL within the IRL framework that generalizes recent advances in maximum entropy deep IRL to online settings. We first established the equivalence between upper bound loss function in equation 25 of the negative log likelihood in equation 5 to moment matching loss of (Swamy et al., 2021). Second, we leveraged sequential second-order Newton optimization to derive an online IRL algorithm by minimizing the moment matching loss function of equation 25 recursively and therefore established key theoretical properties of maximum entropy online deep IRL

RDIRL can learn rewards and cost functions online and greatly outperforms both prior imitation learning and IRL algorithms in terms of steps and samples required to converge. It generally reproduces the batch method's accuracy but in significantly less steps.

The recursive updates in Algorithm 1 require computing the full Hessian of the cost function at each step, which scales quadratically in the number of parameters d_θ. In our experiments this is tractable because the networks are small (two layers of 16 units for continuous control, one layer of 128 units for cognitive radar). For larger networks, well-established approximations such as Gauss-Newton, block-diagonal Hessian approximations (Zhang et al., 2018), or Kronecker-factored preconditioners such as Shampoo (Gupta et al., 2018; Anil et al., 2020) can serve as drop-in replacements for the exact Hessian in equation 39, preserving the recursive structure while reducing computational cost. We plan to explore these extensions in future work.

Acknowledgments

This work was supported in part by the Army Research Laboratory (ARL) under cooperative agreement W911NF2320014, and by the National Institutes of Health (NIH) under grants 7R01DK133605 and R01LM014191.

References

Pieter Abbeel and Andrew Y Ng. Apprenticeship learning via inverse reinforcement learning. In *Proceedings of the twenty-first international conference on Machine learning*, pp. 1, 2004.

Rohan Anil, Vineet Gupta, Tomer Koren, Kevin Regan, and Yoram Singer. Scalable second order optimization for deep learning. *arXiv preprint arXiv:2002.09018*, 2020.

Saurabh Arora, Prashant Doshi, and Bikramjit Banerjee. I2rl: online inverse reinforcement learning under occlusion. *Autonomous agents and multi-agent systems*, 35(1):4, 2021.

Nathanael L Baisa. Derivation of a constant velocity motion model for visual tracking. *arXiv preprint arXiv:2005.00844*, 2020.

Abdeslam Boularias, Jens Kober, and Jan Peters. Relative entropy inverse reinforcement learning. In *Proceedings of the fourteenth international conference on artificial intelligence and statistics*, pp. 182–189. JMLR Workshop and Conference Proceedings, 2011.

G Brockman. Openai gym. *arXiv preprint arXiv:1606.01540*, 2016.

Chelsea Finn, Paul Christiano, Pieter Abbeel, and Sergey Levine. A connection between generative adversarial networks, inverse reinforcement learning, and energy-based models. *arXiv preprint arXiv:1611.03852*, 2016a.

Chelsea Finn, Sergey Levine, and Pieter Abbeel. Guided cost learning: Deep inverse optimal control via policy optimization. In *International conference on machine learning*, pp. 49–58. PMLR, 2016b.

Justin Fu, Katie Luo, and Sergey Levine. Learning robust rewards with adversarial inverse reinforcement learning. *arXiv preprint arXiv:1710.11248*, 2017.

Justin Fu, Anoop Korattikara, Sergey Levine, and Sergio Guadarrama. From language to goals: Inverse reinforcement learning for vision-based instruction following. *arXiv preprint arXiv:1902.07742*, 2019.

Paul Ghanem, Yunus Bicer, Deniz Erdogmus, and Alireza Ramezani. Fast estimation of morphing wing flight dynamics using neural networks and cubature rules. In *2023 62nd IEEE Conference on Decision and Control (CDC)*, pp. 8830–8835. IEEE, 2023.

Paul Ghanem, Ahmet Demirkaya, Tales Imbiriba, Alireza Ramezani, Zachary Danziger, and Deniz Erdogmus. Learning physics informed neural odes with partial measurements. In *Proceedings of the AAAI Conference on Artificial Intelligence*, volume 39, pp. 16799–16807, 2025.

Vineet Gupta, Tomer Koren, and Yoram Singer. Shampoo: Preconditioned stochastic tensor optimization. In *International Conference on Machine Learning*, pp. 1842–1850, 2018.

Tuomas Haarnoja, Aurick Zhou, Pieter Abbeel, and Sergey Levine. Soft actor-critic: Off-policy maximum entropy deep reinforcement learning with a stochastic actor. In *International conference on machine learning*, pp. 1861–1870. Pmlr, 2018.

Dylan Hadfield-Menell, Stuart J Russell, Pieter Abbeel, and Anca Dragan. Cooperative inverse reinforcement learning. *Advances in neural information processing systems*, 29, 2016.

Kathrin Hatz, Johannes P Schloder, and Hans Georg Bock. Estimating parameters in optimal control problems. *SIAM Journal on Scientific Computing*, 34(3):A1707–A1728, 2012.

Simon Haykin. Cognitive radar: a way of the future. *IEEE signal processing magazine*, 23(1):30–40, 2006.

Jonathan Ho and Stefano Ermon. Generative adversarial imitation learning. *Advances in neural information processing systems*, 29, 2016.

HumanCompatibleAI. imitation: Implementation of imitation and inverse rl algorithms. `https://github.com/HumanCompatibleAI/imitation`, 2021. Accessed: 2025-05-14.

Jeffrey Humpherys, Preston Redd, and Jeremy West. A fresh look at the kalman filter. *SIAM review*, 54(4): 801–823, 2012.

Tales Imbiriba, Ahmet Demirkaya, Jindřich Duník, Ondřej Straka, Deniz Erdoğmuş, and Pau Closas. Hybrid neural network augmented physics-based models for nonlinear filtering. In *2022 25th International Conference on Information Fusion (FUSION)*, pp. 1–6. IEEE, 2022.

Wanxin Jin, Zhaoran Wang, Zhuoran Yang, and Shaoshuai Mou. Pontryagin differentiable programming: An end-to-end learning and control framework. *Advances in Neural Information Processing Systems*, 33: 7979–7992, 2020.

Alan J Lipton, Hironobu Fujiyoshi, and Raju S Patil. Moving target classification and tracking from real-time video. In *Proceedings fourth IEEE workshop on applications of computer vision. WACV'98 (Cat. No. 98EX201)*, pp. 8–14. IEEE, 1998.

Anita Matkovic and J Pecaric. A variant of jensen's inequality for convex functions of several variables. *J. Math. Inequal*, 1(1):45–51, 2007.

Timothy L Molloy, Jason J Ford, and Tristan Perez. Online inverse optimal control on infinite horizons. In *2018 IEEE conference on decision and control (CDC)*, pp. 1663–1668. IEEE, 2018.

Timothy L Molloy, Jason J Ford, and Tristan Perez. Online inverse optimal control for control-constrained discrete-time systems on finite and infinite horizons. *Automatica*, 120:109109, 2020.

Timothy L Molloy, Jairo Inga Charaja, Sören Hohmann, and Tristan Perez. *Inverse optimal control and inverse noncooperative dynamic game theory.* Springer, 2022.

Edouard Pauwels, Didier Henrion, and Jean-Bernard Lasserre. Inverse optimal control with polynomial optimization. In *53rd IEEE Conference on Decision and Control*, pp. 5581–5586. IEEE, 2014.

Michael Potter, Shuo Tang, Paul Ghanem, Milica Stojanovic, Pau Closas, Murat Akcakaya, Ben Wright, Marius Necsoiu, Deniz Erdogmus, Michael Everett, et al. Continuously optimizing radar placement with model predictive path integrals. *arXiv preprint arXiv:2405.18999*, 2024.

Anne-Sophie Puydupin-Jamin, Miles Johnson, and Timothy Bretl. A convex approach to inverse optimal control and its application to modeling human locomotion. In *2012 IEEE International Conference on Robotics and Automation*, pp. 531–536. IEEE, 2012.

Nathan D Ratliff, J Andrew Bagnell, and Martin A Zinkevich. Maximum margin planning. In *Proceedings of the 23rd international conference on Machine learning*, pp. 729–736, 2006.

Siddharth Reddy, Anca D Dragan, and Sergey Levine. Sqil: Imitation learning via reinforcement learning with sparse rewards. *arXiv preprint arXiv:1905.11108*, 2020.

Nicholas Rhinehart and Kris M Kitani. First-person activity forecasting from video with online inverse reinforcement learning. *IEEE transactions on pattern analysis and machine intelligence*, 42(2):304–317, 2018.

Stergios I Roumeliotis and George A Bekey. Bayesian estimation and kalman filtering: A unified framework for mobile robot localization. In *Proceedings 2000 ICRA. Millennium conference. IEEE international conference on robotics and automation. Symposia proceedings (Cat. No. 00CH37065)*, volume 3, pp. 2985–2992. IEEE, 2000.

Simo Särkkä and Lennart Svensson. *Bayesian filtering and smoothing*, volume 17. Cambridge university press, 2023.

John Schulman, Filip Wolski, Prafulla Dhariwal, Alec Radford, and Oleg Klimov. Proximal policy optimization algorithms. *arXiv preprint arXiv:1707.06347*, 2017.

Ryan Self, Moad Abudia, and Rushikesh Kamalapurkar. Online inverse reinforcement learning for systems with disturbances. In *2020 American control conference (ACC)*, pp. 1118–1123. IEEE, 2020a.

Ryan Self, Kevin Coleman, He Bai, and Rushikesh Kamalapurkar. Online observer-based inverse reinforcement learning. *IEEE Control Systems Letters*, 5(6):1922–1927, 2020b.

Ryan Self, SM Nahid Mahmud, Katrine Hareland, and Rushikesh Kamalapurkar. Online inverse reinforcement learning with limited data. In *2020 59th IEEE conference on decision and control (CDC)*, pp. 603–608. IEEE, 2020c.

Gokul Swamy, Sanjiban Choudhury, J Andrew Bagnell, and Steven Wu. Of moments and matching: A game-theoretic framework for closing the imitation gap. In *International Conference on Machine Learning*, pp. 10022–10032. PMLR, 2021.

Emanuel Todorov, Tom Erez, and Yuval Tassa. Mujoco: A physics engine for model-based control. In *2012 IEEE/RSJ international conference on intelligent robots and systems*, pp. 5026–5033. IEEE, 2012.

Phillip W Ward, John W Betz, Christopher J Hegarty, et al. Satellite signal acquisition, tracking, and data demodulation. *Understanding GPS: principles and applications*, pp. 153–241, 2006.

Grady Williams, Paul Drews, Brian Goldfain, James M Rehg, and Evangelos A Theodorou. Aggressive driving with model predictive path integral control. In *2016 IEEE International Conference on Robotics and Automation (ICRA)*, pp. 1433–1440. IEEE, 2016.

Zheng Wu, Liting Sun, Wei Zhan, Chenyu Yang, and Masayoshi Tomizuka. Efficient sampling-based maximum entropy inverse reinforcement learning with application to autonomous driving. *IEEE Robotics and Automation Letters*, 5(4):5355–5362, 2020.

Markus Wulfmeier, Peter Ondruska, and Ingmar Posner. Maximum entropy deep inverse reinforcement learning. *arXiv preprint arXiv:1507.04888*, 2015.

Kelvin Xu, Ellis Ratner, Anca Dragan, Sergey Levine, and Chelsea Finn. Learning a prior over intent via meta-inverse reinforcement learning. In *International conference on machine learning*, pp. 6952–6962. PMLR, 2019.

Yiqing Xu, Wei Gao, and David Hsu. Receding horizon inverse reinforcement learning. *Advances in Neural Information Processing Systems*, 35:27880–27892, 2022.

Lantao Yu, Tianhe Yu, Chelsea Finn, and Stefano Ermon. Meta-inverse reinforcement learning with probabilistic context variables. *Advances in neural information processing systems*, 32, 2019.

Siliang Zeng, Chenliang Li, Alfredo Garcia, and Mingyi Hong. Maximum-likelihood inverse reinforcement learning with finite-time guarantees. *Advances in Neural Information Processing Systems*, 35:10122–10135, 2022.

Siliang Zeng, Mingyi Hong, and Alfredo Garcia. Structural estimation of markov decision processes in high-dimensional state space with finite-time guarantees. *Operations research*, 73(2):720–737, 2025.

Han Zhang, Yibei Li, and Xiaoming Hu. Inverse optimal control for finite-horizon discrete-time linear quadratic regulator under noisy output. In *2019 IEEE 58th conference on decision and control (CDC)*, pp. 6663–6668. IEEE, 2019a.

Han Zhang, Jack Umenberger, and Xiaoming Hu. Inverse optimal control for discrete-time finite-horizon linear quadratic regulators. *Automatica*, 110:108593, 2019b.

Huishuai Zhang, Caiming Xiong, James Bradbury, and Richard Socher. Block-diagonal hessian-free optimization for training neural networks. In *International Conference on Learning Representations*, 2018.

Tian Zhao and Timothy L Molloy. Extended kalman filtering for recursive online discrete-time inverse optimal control. *arXiv preprint arXiv:2403.10841*, 2024.

Brian D Ziebart. *Modeling purposeful adaptive behavior with the principle of maximum causal entropy*. Carnegie Mellon University, 2010.

Brian D Ziebart, Andrew L Maas, J Andrew Bagnell, Anind K Dey, et al. Maximum entropy inverse reinforcement learning. In *Aaai*, volume 8, pp. 1433–1438. Chicago, IL, USA, 2008.

A Appendix

B Experiment details

In this section, we list down the implementation details of RDIRL and the baselines. The code is included in the supplementary material. We also report the hyperparameters used in the experiments, the detailed network architectures, training procedures and evaluation procedures used for our experiments.

B.1 Training

In all our experiments, we use MPPI(Williams et al., 2016) as inner policy $q(\tau)$ in our baseline methods. MPPIis a probabilistic model predictive control policy that estimates an optimal action distribution that minimizes an agent's objective cost function. To do so, MPPI samples a number of trajectories and weighs these trajectories depending on how well they minimize the cost function, then updates the mean of its action distribution $q(\tau)$ accordingly. Since MPPI in an online policy , i.e it updates itself every time step, it makes it a natural choice of inner policy for online IRL problems, as we noticed in our preliminary experiments that it is much more stable and has faster convergence that traditional RL methods when implemented inside RDIRL.

The implementation of the baselines (GCL, AIRL,SQIL,ML-IRL and GAIL) are adapted from available public repository (HumanCompatibleAI, 2021).Furthermore, we adapt all the baselines to use MPPI as inner policy alongside our proposed approach. Since the inner policy is not SAC anymore like it was in the original baselines repositories, we tune the parameters of all the adapted baselines using grid search to produce best possible performance. The resulting parameters were used directly in RDIRL. We list the hyper-parameters of all the baselines used in different environments in Table 3. These hyper-parameters were selected via grid search.

Table 3: List of parameters used in each environment.

Environment	Learning rate	Batch size	Reward updates	N_{steps}	Temperature	Horizon	Trajectories
CartPole-v1	1×10^{-4}	150	15	150	1×10^{-3}	50	2000
MountainCar-v0	1×10^{-4}	200	15	200	1×10^{-2}	85	3500
HalfCheetah-v4	1×10^{-4}	200	15	200	1×10^{-2}	50	500
Walker2d	1×10^{-4}	200	15	200	1×10^{-2}	50	500
Hopper	1×10^{-4}	200	15	200	1×10^{-2}	50	500
Cognitive Radar	1×10^{-4}	200	10	200	1×10^{-2}	10	25

In all our experiments, we do multiple passes of parameter updates at the end of each episode using the Adam optimizer for all the baselines for best performance, except in our proposed approach RDIRL, since it is online. The number of passes is listed in the reward function update column of 3. The number of steps executed in each episode in listed in Nsteps column. Temperature,horizon and number of sampled trajectories are MPPI parameters.

PPO (Schulman et al., 2017) is used as the base MaxEnt RL algorithm for the expert policy. Adam is used as the optimizer.

In our proposed RDIRL, we use the same parameters of 3. Additionally, we use $P_{\theta_0} = 10^{-2}I$ and $Q_\theta = 10^{-4}I$ where I is the identity matrix.

B.2 Reward Function and Discriminator Network Architectures

We use the same neural network architecture to parameterize the cost function/reward function/discriminator for all methods. For continuous control task with raw state input, i.e. Cartpole,MountainCar, and the MuJoCo tasks, we use two-layer of MLP with ReLU activation function to parameterized the cost function/discriminator with a hidden size of (16,16). Networks are randomly initialized at the start of each experiment, and all experiments are run on Nvidia-H200 GPU Cluster with 1 GPU per job(seed), with runtimes ranging from 30s/episode for CartPole and 2mins/episode for Walker2d on all benchmarked and competing IRL methods.

B.3 Online Adaptation of competing methods

In this section, we compare our proposed approach, RDIRL, with online-adapted versions of GAIL, AIRL,ML-IRL, and GCL. The online adaptation involves training each competing method using one expert demonstration at a time. Specifically, the loss function of each method is computed using a single observed expert sample at

each time step, followed by an immediate update of the reward function neural network parameters. This process is repeated across the full episode of Nsteps.

As illustrated in Figure 4, our proposed method consistently outperforms the online-adapted baselines. Furthermore, the online adaptation does not significantly improve the performance of the original methods. In the case of Cartpole, it even leads to notable performance degradation and increased instability compared to both the original baselines (GAIL, AIRL,ML-IRL, GCL) and our approach, as shown in Table 4. These results highlight the advantage of our recursive optimization framework in producing more stable and accurate reward functions over naive online adaptation.

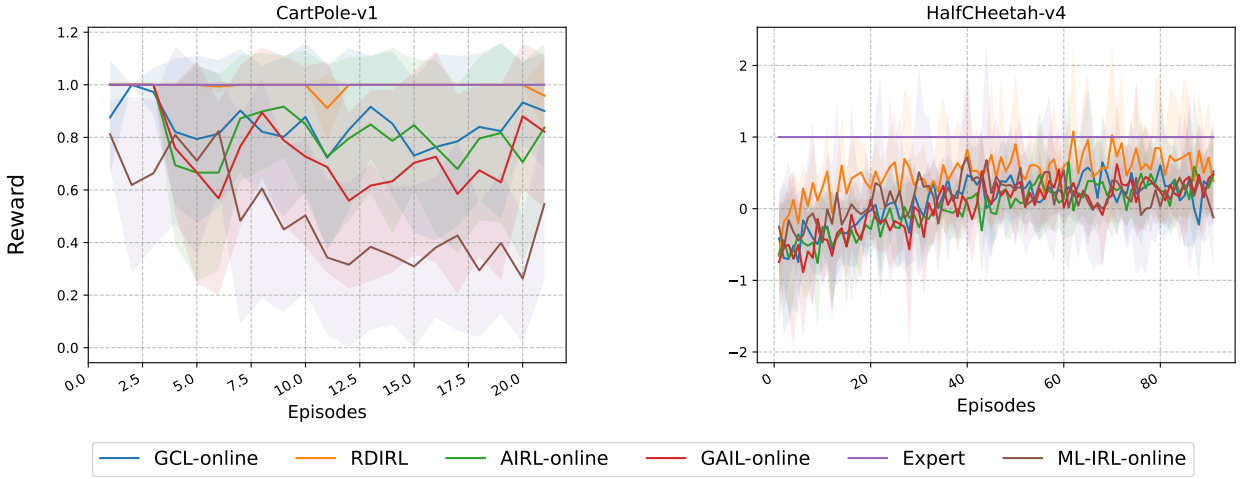

Figure 4: Learning curves for RDIRL and online adaptation methods.

Table 4: Comparison of mean reward values for different Gym environments and online adapted methods.

Methods	CartPole	HalfCheetah-v4
GAIL	0.934 ± 0.058	-0.521 ± 1.15
GCL	0.92 ± 0.09	-0.226 ± 1.27
AIRL	0.953 ± 0.069	-0.54 ± 1.11
GAIL-Online	0.74 ± 0.29	0.02 ± 0.51
GCL-Online	0.84 ± 0.25	0.1 ± 0.53
AIRL-Online	0.81 ± 0.26	0.01 ± 0.49
ML-IRL-Online	0.49 ± 0.29	0.14 ± 0.75
RDIRL (ours)	$\mathbf{0.99 \pm 0.13}$	$\mathbf{0.49 \pm 0.59}$